AIAA 82-4127

Doppler-Aided Low-Accuracy Strapdown Inertial Navigation System

Itzhack Y. Bar-Itzhack,* Daniel Serfaty,† and Yehoshua Vitek‡
Technion—Israel Institute of Technology, Haifa, Israel

This paper presents a covariance analysis of the performance of a Doppler-aided low-accuracy coarsely aligned strapdown inertial navigation system (INS), whose fine alignment takes place automatically in flight. It is shown that the fine alignment in azimuth, which requires turns, consists of in-flight gyro calibration and in-flight gyrocompassing. The spacing of the turns is investigated. The influence of several position fixes is examined, and it is shown that they can replace INS turns. It is also shown that the use of magnetic heading reference reduces system errors but is not necessary for the satisfactory performance of the augmented system. Two suboptimal Kalman filters are designed and evaluated. Their small performance degradation with respect to that exhibited by the optimal filter and their low sensitivity to parameter changes is demonstrated by true covariance simulation runs.

I. Introduction

THE need for an inexpensive midcourse navigation in standoff weapon systems promoted the development of low-cost/low-accuracy strapdown INS (like LCIGS[1,2]) whose gyro constant drift rate is in the range of 1.0 deg/h, and its stability is in the range of 0.1 deg/h in 1 h. While in those systems the strapdown INS is the primary navigational aid, such INS can be installed on other vehicles and be augmented with their own navigation system. The synergistic effect of the augmented systems, whose individual contributions are weighed optimally, is well known from the theory of minimum variance linear estimation.[3]

Many flight vehicles use a Doppler radar navigation system as their standard navigational aid. To upgrade this system one can add to it a low-cost strapdown INS and use a proper Kalman filter to integrate the two systems. Figure 1 illustrates the benefit of such augmentation. The position-error of the Doppler navigation system grows linearly with the distance travelled by the vehicle. If the Doppler system is replaced by a low-accuracy strapdown INS, which is only coarsely aligned, its position-error diverges rapidly with time. When the contribution of both systems is weighed optimally by a Kalman filter along a baseline trajectory, the resulting position-error behaves according to curve b of Fig. 1. (The nature of the baseline trajectory and the time where the peak position-error of the augmented system occurs, will be discussed in the sequel.)

The idea of augmenting a gimballed INS and a Doppler navigation system has been discussed in the past.[4-8] Recently, San Giovanni[9] presented an accuracy performance analysis of a ring laser strapdown attitude and heading reference system that included magnetic heading and airspeed sensors to provide required heading and velocity reference data. He noted that turns of the vehicle on which such a system is mounted generally assist, and in some cases are vital to calibration of many of the system errors.

Using true covariance analysis, the present work investigates the performance of a low-accuracy coarsely aligned Doppler-aided strapdown INS with and without magnetic heading. The main contributions of this work are: 1) investigation and resolution of the effect vehicle turns have on system operation and accuracy, 2) examination of the influence time interval lengths between turns have on system performance, 3) investigation of the weight position fixes have on system operation, and 4) design and analysis of two suboptimal Kalman filters, one for the system with magnetic heading and the other for the system without magnetic heading reference. The efficiency of position fixes and the sensitivity of the suboptimal filters are examined too. Accordingly, the next section presents the error model of the augmented system. Section III presents performance results of the augmented system. An analytic investigation of the importance vehicle turns (turn updates) have in improving system performance is carried out in Sec. IV. Section V deals with the influence of several turn updates and their possible spacing and of position fixes and their spacing. Section VI presents the design of two suboptimal filters and their performance. The main results of this work are summarized in Sec. VII.

II. System Error Model

Figure 2 presents the configuration of the augmented system. The INS is a baro-inertial strapdown system. There are two modes of operation. In the first mode the magnetic heading is used to resolve the Doppler velocity ouput into north and east components from which, then, the corresponding INS computed north and east velocity components are subtracted to form the observables z_1 and z_2 respectively. The indicated magnetic heading is subtracted from the INS indicated heading to form z_3. These observables are processed by an appropriate Kalman filter to yield estimates of the system error states. The latter are then used in either a feedforward or a feedback mode[10] to correct the system-indicated navigation states (Fig. 2 presents the

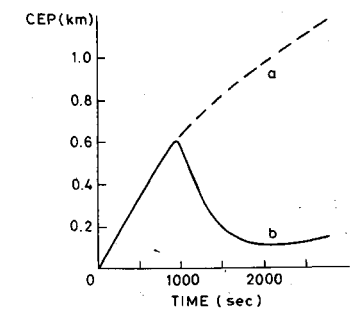

Fig. 1 Horizontal position error growth of a Doppler radar navigation system (curve a) and a Doppler-aided low-accuracy strapdown INS (curve b).

Received June 1, 1981; revision received Nov. 17, 1981.

*Associate Professor, Department of Aeronautical Engineering.
†Graduate Student, Department of Aeronautical Engineering.
‡Research Fellow, Department of Aeronautical Engineering.

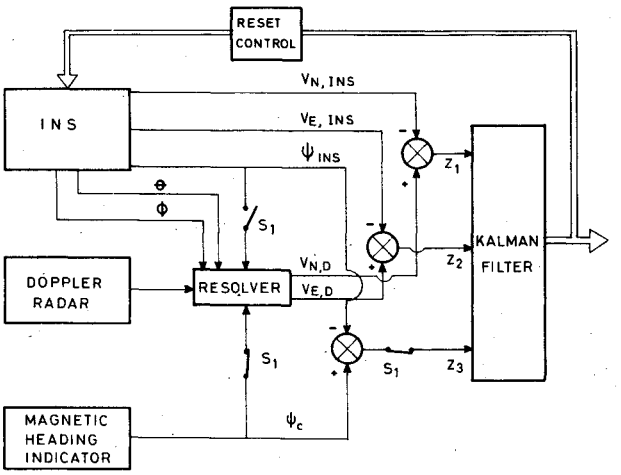

Fig. 2 System configuration (switch positions are according to the first mode of operation).

feedback mode). In the second mode of operation, magnetic heading (or some other heading reference) is used only for preflight coarse azimuth alignment of the INS but it is the INS-indicated heading which is used to resolve the Doppler velocity output. Using the foregoing system description, it can be shown[4,7,11,12] that for the second mode of operation

$$z_1 = -v_N + [(\delta\bar{\theta} - \bar{\phi}) x \bar{V} - \bar{\beta} x \bar{V}]_N + \Delta V_N + n_N \quad (1a)$$

$$z_2 = -v_E + [(\delta\bar{\theta} - \bar{\phi}) x \bar{V} - \bar{\beta} x \bar{V}]_E + \Delta V_E + n_E \quad (1b)$$

where v_N and v_E are, respectively, the errors in the INS-computed north and east velocity components and $\bar{\phi}$ is the vector of attitude difference between the imaginary platform axes[13] and the true local level axis.[14] Similarly, $\delta\bar{\theta}$ is the difference between the computer and local level axes and $\bar{\beta}$ is the boresight error which is, actually, the attitude misalignment error between the Doppler-radar and the aircraft axes. $\bar{V}$ is the true-velocity vector. The quantities ΔV_N and ΔV_E are, respectively, the north and east components of the actual measurement error associated with the Doppler equipment and n_N and n_E are the respective white noise component of these quantities. The subscripts N and E denote, respectively, north and east components in local level coordinates.

For the first mode of operation another measurement is added, namely:

$$z_3 = \delta\psi - (-\phi_D) \quad (2)$$

where $\delta\psi$ is the magnetic heading error and the expressions for z_1 and z_2 are identical to those given in Eqs. (1a) and (1b), respectively, only that ϕ_D, the third component of $\bar{\phi}$, is replaced by $\delta\psi$. (The minus sign in front of ϕ_D in Eq. (2) is due to the fact that the positive direction of ϕ_D is downward.)

The dynamics of the variables which appear in Eqs. (1) and (2) constitute the augmented dynamics equation of the system. The vector $\delta\bar{\theta}$ is expressed in terms of the INS position error as follows:

$$\delta\theta_N = \frac{r_E}{R_E + h} \qquad \delta\theta_E = -\frac{r_N}{R_N + h}$$

$$\delta\theta_D = -\frac{r_E}{R_N + h}\tan L \quad (3)$$

where r_N, r_E and r_D are the components of the INS position error vector expressed in local level coordinates, R_E and R_N are the east and north radii of curvature, h is the altitude and L is the latitude of the vehicle. The dynamics of $\bar{r}$, $\bar{v}$ and $\bar{\phi}$ is expressed by the well-known INS error model.[8,14] The driving function vector of the latter consists of the acclerometer and gyro errors expressed in local level coordinates. These errors are related to the errors of the body-mounted gyros and accelerometers as follows:

$$\begin{bmatrix} \epsilon_L \\ \nabla_L \end{bmatrix} = \begin{bmatrix} D_L^B & 0 \\ 0 & D_L^B \end{bmatrix} \begin{bmatrix} \epsilon_B \\ \nabla_B \end{bmatrix} \quad (4)$$

where ϵ_L and ϵ_B are the vectors of gyro errors expressed in local-level and body coordinates respectively, and ∇_L and ∇_B are the same for accelerometer errors. The matrix D_L^B is the transformation matrix from body to local-level coordinates. The gyro errors which constitute ϵ_B are assumed to be a combination of constant drift, g-sensitive and white noise components. The accelerometer errors are a combination of bias and white noise components which constitute ∇_B.

The Doppler errors ΔV_N and ΔV_E are obtained from ΔV_L where

$$\Delta V_L = D_L^B \Delta V_B \quad (5)$$

The components of ΔV_B contain a constant part and a part which is proportional to the aircraft velocity. Similarly, n_N and n_E are extracted from n_L where

$$n_L = D_L^B n_B \quad (6)$$

and n_B is a white noise vector. The vector $\bar{\beta}$ when resolved in the local-level axes satisfies

$$\beta_L = D_L^B \alpha_B \quad (7)$$

and α_B is a vector of constant boresight error angles in body axes.

The magnetic heading reference error is modeled as a combination of random bias, first order Markov and white noise components.[9]

As a result of the augmentation of the error models of the INS, the Doppler radar and the magnetic heading reference, a system dynamics model is obtained whose state vector contains three position states, three velocity states, three attitude states, three gyro bias states, two gyro g-sensitive states, three accelerometer bias states, three constant Doppler velocity states, three constant boresight error states, a constant, and a Markovian magnetic reference state.

III. Nominal Results

Typical LCIGS and Doppler radar values were chosen as nominal data in this analysis. The values of the initial states are tabulated in Table 1, the values of the system driving noise components are shown in Table 2, and the measurement errors are given in Table 3. The vehicle was flown at a nomimal velocity of 50 m/s to simulate a helicopter flight. The baseline trajectory on which the vehicle was flown consists of a straight and level flight at a 45 deg heading for 900 s, a 90 deg right turn executed in 30 s, a second straight and level flight for another 900 s, a 90 deg left turn executed in 30 s, and a final leg of straight and level flight. The total flight duration is three quarters of an hour.

The main performance characteristics of the augmented navigation system are presented in Fig. 3 where the horizontal error in terms of CEP and the azimuth 1σ estimation error are plotted, both as a function of flight time. These results were obtained for the first mode of operation.

The first turn, which starts at 900 s is, evidently, a key factor in the operation of the augmented system. Without this turn, the performance of the system is as good as the performance of the Doppler navigation system whose horizontal

Table 1 Initial state vector

Notation	Description	Numerical values	Units
r^T	Position error vector	[10, 10, 10]	m
v^T	Velocity error vector	[10, 10, 10][a]	m/s
ϕ^T	Attitude error vector	[5, 5, 5]	deg
ϵ_0^T	Gyro bias error vector	[1.5, 1.5, 1.5]	deg/h
m^T	Gyro g-sensitive drift error vector	[1, 1]	deg/h/g
∇^T	Accelerometer bias	[1, 1, 1]	mg
ΔV_B	Doppler constant velocity error vector	$0.025V+0.10$ $0.0025V+0.10$ $0.0010V+0.05$ V-nominal velocity	m/s m/s m/s
α_B^T	Boresight error vector	[0.3, 0.3, 0.3]	deg
$\delta\psi_0$	Magnetic heading reference constant error	1.5	deg
$\delta\psi_{c1}$	Magnetic heading reference Markov error (correlation time of 1800 s)	1.0	deg

[a]These values were chosen to be unrealistically high in order not to imply too small attitude errors. After the first update, they decrease to their proper values with the right correlations.

Table 2 System driving noise components

Notation	Description	Numerical values	Units
∇_I^T	Accelerometer white noise component	[0.27, 0.27, 0.27]	(m/s)/h$^{1/2}$
ϵ_I^T	Gyro drift white noise component	[0.013, 0.013, 0.013]	deg/h$^{1/2}$
w_ψ	Driving white noise of Markov component of magnetic heading	2.0	deg/h$^{1/2}$

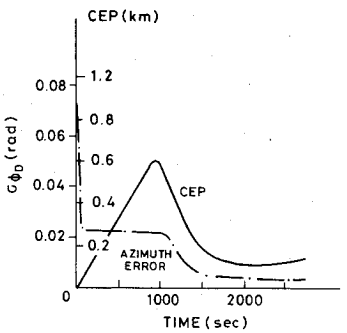

Fig. 3 CEP and azimuth errors of nominal augmented system as function of time.

Table 3 White noise measurement errors

Notation	Description	Numerical values	Units
$\delta\psi_2$	Magnetic heading	15	arc-min
n_B^T	Doppler radar	[0.2, 0.2, 0.2]	m/s
ΔR^T	External position information (when available)	[20, 20]	m

position error as a function of time is shown in Fig. 1 (curve a). It is the reduction of the azimuth error, beginning at the turn, which completes the INS alignment and thus turning it into an acceptable navigation system whose augmentation with the Doppler radar yields an improved navigation device. The question why hitherto nothing happened and azimuth alignment begins only after the turn, is important to the understanding of the operation of the system. This question is addressed in the next section.

IV. Analytic Investigation of the Turn Update

INS azimuth self-alignment (as opposed to optical alignment) can be achieved through either transfer alignment or gyrocompassing. The difference between the two can be briefly explained as follows. In transfer alignment, some vector is measured by both the INS and a certain reference system. The vector is thus coordinatized in both systems. The difference between the corresponding components of this vector in the two systems is a measure of the misalignment error. In gyrocompassing, though, the INS azimuth misalignment, in collaboration with the north component of the sum of Earth rate and the rate of change of the longitude, cause a growing tilt about the east axis, which in turn yields a growing north velocity-error component. A measure of this error component is obtained from the comparison of the INS north velocity with that of some reference system. (Further details are given in Ref. 15.)

Although vehicle maneuvers enhance azimuth observability during transfer alignment,[15] the notion that transfer alignment occurs during the turn is ruled out at the outset. The reason for rejecting this explanation stems from the fact that in transfer alignment the final alignment can be only as good as that of the reference system[16] which, in our case, is determined by the magnetic heading reference whose accuracy is around 1.8 deg. The turn itself adds no additional information on the azimuth misalignment. This conclusion can be arrived at analytically, too. Consider point P_0 in Fig. 4, which is a point close to the beginning of the turn. At this point, where the flight time is 900 s, almost all of the tilt error has been already estimated and removed. For simplicity it is assumed that the position error is zero, that the Doppler radar is perfect and its boresight errors are negligible. For, if under such tight conditions,the azimuth error is unobservable, it is surely so for more lax conditions. Under these conditions the measurement equations of the first mode of operation, that is, Eqs. (1) and (2) can be reduced to the following:

$$z_{1,0}=-v_{N0}-V_{E0}\cdot\delta\psi \qquad z_{2,0}=-v_{E0}+V_{N0}\cdot\delta\psi$$

$$z_{3,0}=\phi_D+\delta\psi \tag{8}$$

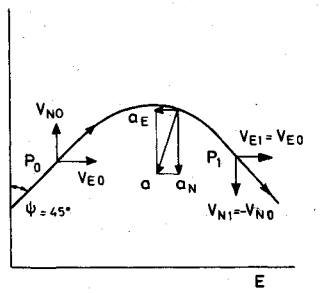

Fig. 4 Velocity and acceleration components at the turn.

where the subscript *0* denotes variables at point P_0. From the deterministic point of view, there are four unknowns; namely, ϕ_D, $\delta\psi$, v_{N0} and v_{E0} with only three equations, thus the system of equations cannot be resolved. From the stochastic point of view, it is observed that repeated measurements and updates on this leg do not change the lack of stochastic observability [3,15,17] of ϕ_D.

To show that the turn does not yield immediate information to enhance the observability of ϕ_D, consider the following development. During the turn the errors ϕ_D and $\delta\psi$ remain basically constant. However, the INS velocity error components v_N and v_E do vary. It can be easily shown[15] that essentially they vary according to the following dynamics equations

$$\dot{v}_E = -a_N\phi_D \qquad \dot{v}_N = a_E\phi_D \tag{9}$$

Since ϕ_D stays constant, Eqs. (9) can be integrated to yield

$$v_{E1} = v_{E0} - \phi_D\int_{t_0}^{t_1} a_N dt \qquad v_{N1} = v_{N0} + \phi_D\int_{t_0}^{t_1} a_E dt \tag{10}$$

where t_0 and t_1 denote the time at P_0 and P_1 respectively, and the subscript 1 denotes variables at point P_1. The integrals in Eqs. (10) are equal to the change in the nominal velocity components between points P_0 and P_1 hence

$$\int_{t_0}^{t_1} a_N dt = V_{N1} - V_{N0} \qquad \int_{t_0}^{t_1} a_E dt = V_{E1} - V_{E0} \tag{11}$$

but from Fig. 4

$$V_{N1} = -V_{N0} \qquad V_{E1} = V_{E0} \tag{12}$$

thus Eqs. (11) become

$$\int_{t_0}^{t_1} a_N dt = -2V_{N0} \qquad \int_{t_0}^{t_1} a_E dt = 0 \tag{13}$$

Substituting Eqs. (13) into Eqs. (10) yields

$$v_{E1} = v_{E0} + 2V_{N0}\phi_D \qquad v_{N1} = v_{N0} \tag{14}$$

Now, similarly to Eqs. (8), and using the previous assumptions, the measurement equations at point P_1, which is after the completion of the 90 deg turn, are

$$z_{1,1} = -v_{N1} - V_{E1}\cdot\delta\psi \qquad z_{2,1} = -V_{E1} + V_{N1}\cdot\delta\psi$$
$$z_{3,1} = \phi_D + \delta\psi \tag{15}$$

With the aid of Eqs. (12) and Eqs. (14) these measurements can be expressed in terms of the previous measurements as follows:

$$z_{1,1} = -v_{N0} - V_{E0}\delta\psi$$
$$z_{2,1} = -v_{E0} - 2V_{N0}\phi_D - V_{N0}\delta\psi$$
$$= -v_{E0} + V_{N0}\delta\psi - 2V_{N0}(\phi_D + \delta\psi)$$
$$z_{3,1} = \phi_D + \delta\psi \tag{16}$$

A comparison between Eqs. (16) and (8) yields

$$z_{1,1} = z_{1,0} \qquad z_{2,1} = z_{2,0} - 2V_{N0}z_{3,0} \qquad z_{3,1} = z_{3,0} \tag{17}$$

that is, the new measurements at P_1 are a linear combination of the measurements at P_0. No additional information has been added, and we are still left with only three independent equations and four unknowns. In conclusion, the turn added no new information on the INS azimuth alignment. Note that for simplicity we chose the initial heading to be 45 deg. The preceding analysis can, of course, be extended to include an arbitrary initial heading.

The preceding discussion raises an important point for the analyst. In a covariance simulation, the change in v_N and v_E due to a_E and a_N, which is given here in its simplest form by Eqs. (10), is modeled, though in a more elaborate fashion, in the dynamics equation of the INS error propagation.[8,14] On the other hand, the nominal velocity components, which are also functions of v_N and v_E and which are the entries of the measurement matrix [see Eqs. (9) and (16)] are known and entered into the measurement matrix directly. If due to computation inaccuracies the computed transition matrix, and consequently the propagated covariance matrix, are inaccurate, the relations expressed in Eqs. (11) are not fulfilled exactly. Therefore, there is a slight incompatibility between the covariance matrix and the corresponding measurement matrix. Hence, the relationship between the measurements at P_0 and those at P_1 is, erroneously, not quite as given in Eqs. (17). Consequently, this slight mismatch renders a certain degree of azimuth observability which does not exist in reality. For this reason a covariance analysis, if not executed carefully, yields overly optimistic results after turns.

After rejecting the possibility that vehicle turns enhance system operation through transfer alignment, we consider now the possibility that it is gyrocompassing that improves system performance. According to this assumption, during the first leg of the flight the equivalent north gyro drift is observable. Therefore, its value is estimated or, in other words, the equivalent north gyro is calibrated during the first straight and level flight segment. During this time the equivalent east gyro drift is unobservable and cannot be calibrated. It is well known that the east gyro constant drift rate sets a lower limit on ϕ_D. Therefore, as long as the straight and level flight continues, ϕ_D remains on a constant high level. The 90 deg turn places the equivalent north gyro of the first leg in the east direction, and the equivalent east gyro in the north-south direction replacing the task of the two equivalent gyros. The new equivalent east gyro is now a calibrated gyro; that is, its constant drift has been calibrated out considerably. This reduces the lower limit that ϕ_D can reach through gyrocompassing, which enables the estimation of the azimuth misalignment. With the reduction of ϕ_D the observability of other INS errors increases, their values are reduced and the INS becomes a higher quality system.

What is the evidence to support this calibration and gyrocompassing explanation of the influence vehicle turns have on system performance? To examine whether calibration indeed takes place, let the vehicle fly north or east and observe the estimation error of the constant drift rates of the north-south and east-west gyros. In this case, the north and east

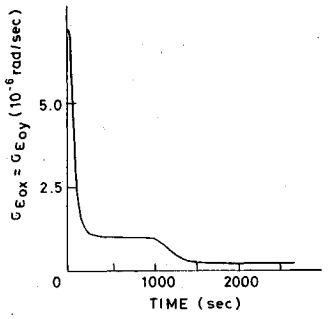

Fig. 5 Reduction of the estimation error of the constant drift rate of the horizontal strapdown gyros.

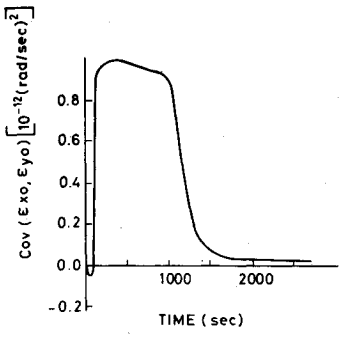

Fig. 6 Behavior of the cross-correlation between the estimation errors of the constant drift rate of the horizontal strapdown gyros.

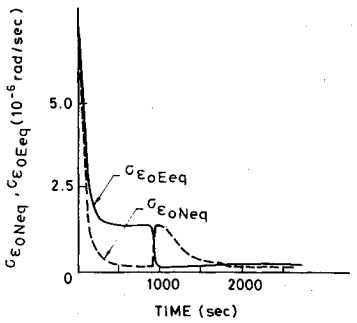

Fig. 7 Behavior of the estimation error of the constant drift rate of the equivalent north and east gyros.

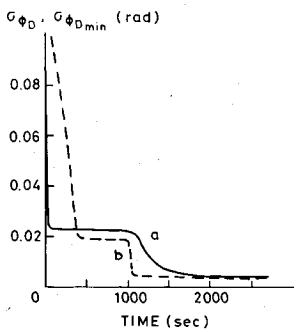

Fig. 8 $\sigma_{\phi D}$ (curve a) and its lower bound (curve b).

equivalent gyros coincide with the strapdown gyros whose drift errors are included in the state vector. The reduction of the north gyro drift prior to the turn and its substitution with east gyro drift after the turn is evident from the simulation results. What happens, though, when the azimuth of the first leg is neither in the north-south nor in the east-west direction. In this case the equivalent north and east gyro drifts are a linear combination of the strapdown gyros and are not modeled directly in the state of the system. To examine the calibration effect in this case note that

$$\epsilon_{0Neq} = \epsilon_{0x}\cos\psi - \epsilon_{0y}\sin\psi \qquad \epsilon_{0Eeq} = \epsilon_{0x}\sin\psi + \epsilon_{0y}\cos\psi \tag{18}$$

where ϵ_{0Neq} and ϵ_{0Eeq} are, respectively, the equivalent north gyro constant drift and equivalent east gyro constant drift. Similarly ϵ_{0x} and ϵ_{0y} are, respectively, the constant drifts of the roll axis and the pitch axis strapdown gyros. Using Eqs. (18) it can be easily shown that the standard deviations are given by

$$\begin{aligned}\sigma_{\epsilon 0Neq} &= [\sigma^2_{\epsilon 0x}\cdot\cos^2\psi + \sigma^2_{\epsilon 0y}\cdot\sin^2\psi - 2\sigma_{\epsilon 0x\epsilon 0y}\cdot\sin\psi\cos\psi]^{1/2}\\ \sigma_{\epsilon 0Eeq} &= [\sigma^2_{\epsilon 0x}\cdot\sin^2\psi + \sigma^2_{\epsilon 0y}\cdot\cos^2\psi + 2\sigma_{\epsilon 0x\epsilon 0x}\cdot\sin\psi\cos\psi]^{1/2}\end{aligned} \tag{19}$$

Consider now the baseline trajectory where for the first leg $\psi = 45$ deg. In this case Eqs. (19) become

$$\begin{aligned}\sigma_{\epsilon 0Neq} &= [\tfrac{1}{2}(\sigma^2_{\epsilon 0x} + \sigma^2_{\epsilon 0y}) - \sigma_{\epsilon 0x\epsilon 0y}]^{1/2}\\ \sigma_{\epsilon 0Eeq} &= [\tfrac{1}{2}(\sigma^2_{\epsilon 0x} + \sigma^2_{\epsilon 0y}) + \sigma_{\epsilon 0x\epsilon 0y}]^{1/2}\end{aligned} \tag{20}$$

On the first leg both $\sigma_{\epsilon 0x}$ and $\sigma_{\epsilon 0y}$ decrease in an identical manner as shown in Fig. 5 whereas $\sigma_{\epsilon 0x\epsilon 0y}$ grows as shown in Fig. 6. The net effect as expressed by Eqs. (20) is shown in Fig. 7. Observe that the large estimation error of ϵ_{0Neq} is indeed calibrated out. It reaches a steady state at about 500 s into the flight. Even the initial estimation error ϵ_{0Eeq} goes down, but it reaches a steady state, which is much higher than required. (The reason for this initial reduction of $\sigma_{\epsilon 0Eeq}$ will be discussed in the sequel.) During the turn at 900 s, the azimuth angle changes from 45 deg to 135 deg. Using the new value of ψ in Eqs. (19) yields

$$\begin{aligned}\sigma_{\epsilon 0Neq} &= [\tfrac{1}{2}(\sigma^2_{\epsilon 0x} + \sigma^2_{\epsilon 0y}) + \sigma_{\epsilon 0x\epsilon 0y}]^{1/2}\\ \sigma_{\epsilon 0Eeq} &= [\tfrac{1}{2}(\sigma^2_{\epsilon 0x} + \sigma^2_{\epsilon 0y}) - \sigma_{\epsilon 0x\epsilon 0y}]^{1/2}\end{aligned} \tag{21}$$

A comparison between Eqs. (20) and (21) reveals how the physical interchange between the north and east equivalent gyros is expressed analytically. Since from Fig. 5 it is clear that neither $\sigma_{\epsilon 0x}$ nor $\sigma_{\epsilon 0y}$ change appreciably during the turn and since, from Fig. 6, the same can be said about $\sigma_{\epsilon 0x\epsilon 0y}$, it is clear that the amount by which $\sigma^2_{\epsilon 0Eeq}$ decreases during the turn is nearly $2\sigma_{\epsilon 0x\epsilon 0y}$. It is concluded, therefore, that when the first leg is parallel neither to the N axis nor to the E axis, the cross correlation between ϵ_{0x} and ϵ_{0y}, which is built during the first leg, is essential to the reduction of $\sigma_{\epsilon 0Eeq}$.

To show that this calibration is followed by gyrocompassing consider the lower bound which ϕ_D can reach through gyrocompassing. It is well known from the INS error equations that

$$|\phi_D| \geq |\epsilon_{0E}|/(\Omega + \dot{\lambda})\cos L \tag{22}$$

therefore

$$\sigma_{\phi D} \geq \sigma_{\epsilon 0Eeq}/(\Omega + \dot{\lambda})\cos L \tag{23}$$

Curve b of Fig. 8 is a plot of the right-hand side of Eq. (23); that is, of the lower bound of $\sigma_{\phi D}$ as a function of time. Curve a is a plot of $\sigma_{\phi D}$ itself as a function of time. It is seen that after the first update, $\sigma_{\phi D}$ goes down to the value of the heading reference, which is a part of the "master" reference system. This is why $\sigma_{\phi D}$ in this region is lower than the lowest bound attainable through gyrocompassing. In fact, here it is the better quality of azimuth information, which is the source for the calibration (the decrease) of the equivalent east gyro constant drift rather than vice versa. When, at about 400 s, the equivalent east gyro constant drift reaches its steady-state value, which is compatible with $\sigma_{\phi D}$, it stays constant while $\sigma_{\phi D}$ is practically unchanged. After the turn, though, the lower bound on $\sigma_{\phi D}$ is drastically reduced with the reduction of σ_{0Eeq}. Then, $\sigma_{\phi D}$ starts moving down to its lower bound on a curve typical, in its time behavior, to a gyrocompassing

Table 4 The effect of turn spacing

Case no.	Time of first turn, s	Time of second turn, s	Azimuth error σ_{ϕ_D}, mrad			Position error (CEP), m	
			Initial[a]	Before second turn	Final	Maximal	Final
1	100	1800	23	25.3	4.0	592	109
2	200	1800	23	12.7	4.0	379	96
3	400	1800	23	7.3	3.7	320	89
4 (Baseline)	900	1800	23	5.1	4.0	710	140
5	1400	1800	23	4.7	3.5	1077	202
6	200	400	23	9.3	8.0	237	218
7	200	600	23	8.9	6.7	237	194
8	400	900	23	8.0	5.9	320	171

[a] After the first update where reference heading updates ϕ_D.

curve. From the fact the σ_{ϕ_D} hunts but never decreases below its lower bound set in *gyrocompassing* and from the time behavior of the decrease of σ_{ϕ_D} after the turn, it is concluded that it is a gyrocompassing process that improves the estimation of ϕ_D after the calibration of the north gyro constant drift rate, and the exchange of the north and the east equivalent gyros.

If this explanation is correct, then there is no need for the whole vehicle to turn since it is enough to turn just the INS case about the azimuth axis. Indeed, when the covariance program simulates a straight and level flight along which the INS is turned at the times at which the whole vehicle turned when it was flown on the baseline trajectory, the behavior of σ_{ϕ_D} as well as of $\sigma_{\epsilon 0 Eeq}$ is almost identical to their behavior on the baseline trajectory. The position error propagation is also similar to its behavior on the baseline trajectory. The only difference is that after its fast decrease, which follows the first turn, the position error starts diverging slowly. This is due to the fact that the rotation of the velocity vector which takes place on the baseline trajectory, enables the estimation of the Doppler velocity error components ΔV_{Bx} and ΔV_{By} while this does not happen on the straight and level flight. At any rate, calibration and gyrocompassing occur here too, as it should.

V. Influence of Several Turn Updates and Position Fixes

Turn updates do not necessarily require the turn of the entire vehicle. Following the preceding explanation, it is clear that for a turn update it is sufficient to turn the sensor cluster only. Even so, one is interested in knowing how often turn updates have to be executed. It has been found that for all practical purposes two such updates suffice. The question is, then, when to execute them. Obviously, if the first turn is carried out before calibration is completed, the successive gyrocompassing is not very effective after the first turn. In such cases, the second turn becomes more effective than on the baseline trajectory. To examine the effect turn spacing has on performance, several covariance simulations were run. The basic features of the baseline trajectory were kept in those runs with the only exception that the two turns were executed at different time points. The results of those runs are summarized in Table 4.

The following conclusions are derived from Table 4:

1) Enough time has to elapse before the first turn becomes effective. In this system the optimal time for the first turn is 400 s.

2) If the time of the first turn is sufficiently large, the effect of the second turn is minimal. Then, however, one has to live with large position errors for a longer time.

3) Lowest final position error is achieved when the first turn is executed at 400 s.

4) Lowest final azimuth error is achieved when the first turn is executed late in the mission.

5) The efficiency of the second turn update increases with time between turns.

Table 5 Error growth (in percent) with respect to the optimal filter when using a suboptimal filter

Resultant error in	At $t=900$ s (before the turn)		At $t=2700$ s (at end of flight)	
	SOF1	SOF2	SOF1	SOF2
r_N	3.1	1.4	6.5	4.8
r_E	3.1	1.4	6.7	5.0
v_N	2.0	1.3	5.8	4.1
ϕ_N	0.5	0.1	9.0	7.0
ϕ_E	0.2	0.0	4.6	4.1
ϕ_D	3.6	1.6	7.1	4.9

The influence of discrete position fixes was examined too. Two cases were simulated. In the first case, high frequency Doppler updates were performed as usual and, in addition, low frequency position updates were performed too. The second case included a turn update, in addition to the two kinds of updates of case one. The results of the first case are typical to those of a position updated ordinary INS (see, for example, Figs. 8 and 9 in Ref. 18). As for the second case, the simulation was performed on a trajectory which, like the baseline trajectory, started with a 45 deg straight and level flight then a position update took place at 180 s, a 90 deg right-hand turn was performed at 360 s, and a second position update took place at 540 s. The simulation was terminated at 1200 s. The accuracy of the fix was 20 m in the north direction and 20 m in the east direction. This updating schedule yielded final CEP of 30 m, and a final azimuth error of 4 mrad (1σ). It is concluded, therefore, that if within 30 km of the takeoff point there are identifiable landmarks, or there is another means for position fix whose RSS is around 30 m, one turn update suffices, and a good quality augmented navigation system is obtained after just 10 min of flight time.

VI. Suboptimal Filter Design

The advantages of using a suboptimal rather than an optimal Kalman filter are well documented.[3,8] Of the several possible categories of suboptimal filters (SOF), the approach of reducing the order of the SOF was chosen in this work. To meet this end, the observability of the elements of the state vector of the "truth model" was examined. It was found that the estimation error of ϵ_{0D}, m, and ΔV_{By} was hardly reduced (i.e., the reduction was between 0 to 30%). The estimation error of ∇_z, $\delta\psi_0$, and $\delta\psi_1$ was reduced moderately (i.e., 30 to 60%). These states were, therefore, candidates for elimination from the state of the SOF. Because of the weak correlation between the vertical and the horizontal channels of the INS, and due to the barometric damping of the vertical channel, its states were eliminated from the SOF state altogether. Adopting these considerations, several reduced order SOF's were evaluated. The evaluation tool was a covariance

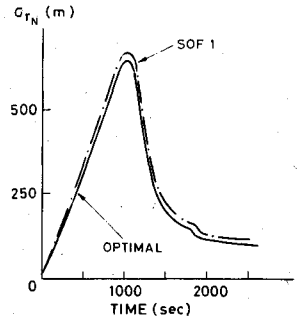

Fig. 9 Time histories of σ_{rN} when the optimal filter is used and when SOF1 is used.

Table 6 Final errors when using the optimal filter, SOF1 and SOF2

	Filter		
Final error in	Optimal	SOF1	SOF2
CEP, m	140	150	147
Tilt, mrad	0.085	0.092	0.090
Azimuth, mrad	4.0	4.30	4.21

simulation program that runs simultaneously the SOF filter and the truth model[19,20] and yields the true covariance of the actual estimation error, which is obtained when using the SOF to estimate the state of the "truth model." As a result of the evaluation, two reduced order SOF's were chosen; one for the first mode of operation, and one for the second. The state of the SOF for the first mode, which is denoted by SOF1, is

$$x^{*T} = [r_N, r_E, v_N, v_E, \phi_N, \phi_E, \phi_D, \epsilon_{0x}, \epsilon_{0y}, \epsilon_{0z}, \nabla_x, \nabla_y, \Delta V_{Bx}, \Delta V_{By}] \tag{24}$$

and that for the second mode of operation, which is denoted by SOF2, consists of the same plus $\delta\psi_1$. Table 5 presents the performance of the two filters with respect to the optimal one. Figure 9 presents the time histories of σ_{rN} for both SOF1 and the optimal filter. Finally, Table 6 presents a comparison between the final errors of the most important navigation variables when SOF1, SOF2, and the optimal filter are used. An error sensitivity for SOF1 was carried out. Accordingly, the filter used the nominal parameters, whereas the parameters in the "truth model" were changed. The suboptimal filter exhibited low sensitivity to a wide range of changes. This in contrast with the well-known[3] high sensitivity of the optimal filter which was verified too in a separate sensitivity analysis.

VII. Conclusions

It is concluded that the augmentation of a low-cost coarsely aligned strapdown INS with a Doppler radar constitutes a very good navigation and attitude reference system which, in our case, yields a few mrad azimuth error and a few hundred meters of position error after 2700 s of flight time. This is true only at the later phases of the flight when error reduction takes place. One condition for the satisfactory performance of the augmented system is the ability to turn the INS in azimuth, at least at two points along the flight path. During the initial part of the flight, the equivalent north gyro is being automatically calibrated, and then after the first 90 deg turn it becomes the equivalent east gyro. At this point gyrocompassing commences, which brings down the azimuth as well as the other navigation errors. A second turn helps in completing this process. INS turns can be replaced by several position updates. A suboptimal filter can be used to augment the two systems. It yields very good results; the errors are very close to those generated when the optimal filter is used and the filter is quite insensitive to parameter changes. A reference heading improves the performance of the system but is not necessary. A turn of the INS alone can replace the turning of the whole vehicle since gyro calibration and gyrocompassing occur this way too. Better position results, though, occur when the whole vehicle turns since the turning of the velocity vector enables the estimation of the Doppler horizontal error components.

Acknowledgments

This research was supported by TAMAM—Precision Instrument Industries, Division of Israel Aircraft Industries, Ltd.

References

[1] Gilmore, J. P., "Modular Strapdown Guidance Unit with Embedded Microprocessor," *Journal of Guidance and Control,* Vol. 3, Jan.-Feb. 1980, pp. 3-10.

[2] Kraemer, J. W., Roessler, N. J., and Brandin, D. M., "In-Flight Alignment/Calibration Techniques for Unaided Tactical Guidance," *Proceedings of the National Aerospace and Electronics Conference,* Dayton, Ohio, 1978, pp. 705-711.

[3] Gelb, A., (ed.), *Applied Optimal Estimation,* MIT Press, Cambridge, Mass., 1974.

[4] Nash, R. A., Jr., D'Appolito, J. A., and Roy, K, J., "Error Analysis of Hybrid Aircraft Inertial Navigation Systems," AIAA Paper 72-848, *AIAA Guidance and Control Conference,* Aug. 1972.

[5] Lochrie, W. D., "The Evaluation of Autonomous Navigation Systems for Cruise Vehicles," AIAA Paper 73-874, Aug. 1973.

[6] Heller, W. G., "Models for Aided Inertial Navigation System Sensor Errors," The Analytic Sciences Corp., Reading, Mass. TASC TR-312-3, Feb. 1975.

[7] Kasper, J. F., Jr. and Nash, R. A., Jr., "Doppler Radar Error Equations for Damped Inertial Navigation System Analysis," *IEEE Transactions on Aerospace and Electronic Systems,* Vol. AES-11, July 1975, pp. 600-607.

[8] Maybeck, P. S., *Stochastic Models, Estimation and Control,* Vol. 1, Academic Press, New York, 1979.

[9] San Giovanni, C., Jr., "Performance of a Ring Laser Strapdown Attitude and Heading Reference for Aircraft," *Journal of Guidance and Control,* Vol. 2, July-Aug. 1979, pp. 320-327.

[10] Huddle, J. R., "Application of Kalman Filtering Theory to Augmented Inertial Navigation Systems," in *Theory and Applications of Kalman Filtering,* NATO AGARDograph 139, AD-704 306, Feb. 1970, pp. 236-268.

[11] Benson, D. O., Jr., "A Comparison of Two Approaches to Pure-Inertial and Doppler-Inertial Error Analysis," *IEEE Transactions on Aerospace and Electronic Systems,* Vol. AES-11, July 1975, pp. 447-455.

[12] Bar-Itzhack, I. Y., "INS Position-Error and Velocity-Error Models," Technical Report No. TAE 396, Technion, Dept. of Aeronautical Engineering, Haifa, Israel, Feb. 1980.

[13] Weinreb, A. and Bar-Itzhack, I. Y., "The Psi-Angle Error Equation in Strapdown Inertial Navigation Systems, " *IEEE Transactions on Aerospace and Electronic Systems,* Vol. AES-14, May 1978, pp. 539-542.

[14] Leondes, C. T., (ed.), *Guidance and Control of Aerospace Vehicles,* McGraw-Hill, New York, 1963, Chap. 2.

[15] Bar-Itzhack, I. Y. and Porat, B., "Azimuth Observability Enhancement During Inertial Navigation System In-Flight Alignment," *Journal of Guidance and Control,* Vol. 3, July-Aug. 1980, pp. 337-344.

[16] Bar-Itzhack, I. Y. and Malove, E. F., "Accurate INS Transfer Alignment Using a Monitor Gyro and External Navigation Measurements," *IEEE Transactions on Aerospace and Electronic Systems,* Vol. AES-16, Jan. 1980, pp. 53-65.

[17] Bryson, A. E., Jr. and Ho, Y. C., *Applied Optimal Control,* John Wiley, New York, 1975, pp. 369, 370.

[18] Gelb, A. and Sutherland, A. A., Jr., "Software Advances in Aided Inertial Navigation Systems," *Navigation: Journal of the Institute of Navigation,* Vol. 17, No. 4, Winter 1970-71, pp. 358-369.

[19] D'Appolito, J. A., "The Evaluation of Kalman Filter Designs for Multisensor Integrated Navigation Systems," TASC TR-183-1, The Analytic Sciences Corp., Reading, Mass., Jan. 1971.

[20] Medan, Y. and Bar-Itzhack, I. Y., "Error and Sensitivity Analysis Scheme of a New Data Compression Technique in Estimation," *Journal of Guidance and Control,* Vol. 4, Sept.-Oct. 1981, pp. 510-517.